



# Full-Field Thermographic Analysis for Fatigue Damage Detection of Composite Specimens

Alessandra Pirinu<sup>(✉)</sup> and Francesco Panella

Department of Engineering for Innovation, University of del Salento, Viale per Monteroni,  
73100 Lecce, LE, Italy  
alessandra.pirinu@unisalento.it

**Abstract.** For composite materials, thermographic techniques have been successfully employed as a suitable monitoring procedure based on the thermo-elastic stress analysis, combined with dissipative effects in full-field data processing approaches for the rapid detection of critical stressed zones, where the delamination initiation or fiber cracks arise under cyclic loads, with the simultaneous aim to establish, at the earliest time, damage phenomena evolving and turning to significant magnitude.

The present work briefly resumes different case of studies with fatigue characterization under tensile load of composite samples also in presence of notched holes, subjected to damage evolution in different ways, as function of load intensity and endurance. An interesting hybrid methodology for damage evaluation during cyclic loads is proposed through the combination of real-time thermographic recording with the consolidated and robust stiffness analysis (compliance analysis). Raw thermal and processed data are employed for a qualitative analysis of critical zones and proper damage indication before failure. In addition, proposed thermal parameters and experimental compliance data seem to indicate good correlation for damage detection in different cases.

**Keywords:** Composite material · Damage prediction · Fatigue test · Industrial element · Thermographic monitoring

## 1 Introduction

In recent years, improvement of data-processing methods for thermographic acquisitions has been studied for reliable damage monitoring and defects detection through different strategies on flat composite parts. Specific physical and mechanical property makes these materials very attractive to the transportation industry, i. e. lightweight, elevated stiffness and a good resistance against corrosion and fatigue, reducing both the fuel consumption and the emissions of greenhouse gases [1, 2]. However, an important research interest is focused on fatigue behavior and in presence of notch or pre-existing defects (i.e. manufacturing or impact damages) that represents the more expensive and complex characterization of innovative materials due to long time and difficult experimental campaign. During service life, damage mechanisms could occur in mechanical structure

under static and dynamic loads and damage evolution process requires a suitable monitoring strategy by means of non-destructive techniques [3, 4]. Nowadays, the continuous improvement of Non-destructive testing (NDT) and the advanced solutions of Structural health monitoring (SHM) represent the major challenge for advanced industrial materials to improve structural reliability and integrity procedures reducing time and cost for mechanical characterization of metals and composite [5, 6].

Among different monitoring techniques, the Thermoelastic Stress Analysis [7] (TSA) represents a well-established no-contact method for stress evaluation of isotropic or orthotropic engineering components [8, 9]. Specifically, in TSA technique, small reversible temperature change associated with the thermoelastic effect are analyzed in a component subjected to cyclic load employing a sensitive infrared camera [7, 8]. In addition, recent research highlights the damage detection capability and monitoring potentials of micro-bolometric infrared camera showing the more cost effective and commercial availability solutions for TSA approach without an expensive thermographic equipment [7, 10].

In this work, three different Carbon Fiber/epoxy (CFRP) composite specimens are tested under tension-tension cyclic loading to study fatigue behaviour in presence of delamination initiation, wrinkle defect or junction hole. These composite elements consist of thick beams and Flat Open Hole (FOH) elements in presence or in absence of wrinkled zones, realized in pre-preg autoclave curing or through the Liquid Resin Infusion technology. Experimental tests are in-real time monitored with thermal acquisitions, investigating the proposed damage parameters in critical zones before failure and correlated to fatigue residual life expectancies. However, the present proposed work efforts consist of better damage localization (well observed with visual and thermographic inspection) and quantification of propagation severity, compared with the well-established compliance analysis.

## 2 Materials and Methods

### 2.1 CFRP Elements

In this section, cyclic tests were performed on different type of CFRP elements. The first series consist of two flat rectangular Open Hole specimens [Dim.  $304 \times 39 \times 4.5$  mm] with central hole of 6.35 mm nominal diameter, denoted as W-type specimens and showed in Fig. 1 (a). These samples are denoted 'W type' specimens and manufactured with autoclave curing process employing unidirectional pre - preg IMS /977 -2 UD TAPE with layers of 0.186 mm nominal thickness and lamination sequence  $[+45, +90, 0, 0, -45, 0, 0, -45, 0, 0, +90, +45]_s$  introducing an artificial wrinkle in the reduced section pressing several layers of calibrated thicknesses during cure process. Before curing process, the stacked laminate is pressed in the critical central section to reproduce an artificial wrinkle with specific depth and width during curing phase, with geometric parameters of artificial wrinkle shape illustrated at right side in Fig. 1(a).

The second case of study consists of two specimens Carbon-Epoxy composite plates [Dim.  $130 \times 39 \times 6.78$  mm], denoted as 'B-type' samples. These CFRP elements of simple geometry were laminated with a specific lay-up  $[+45, -45, 0, +90]_{4s}$  symmetrically arranged in a quasi-isotropic layout with 32 plies of unidirectional BNFC-24k

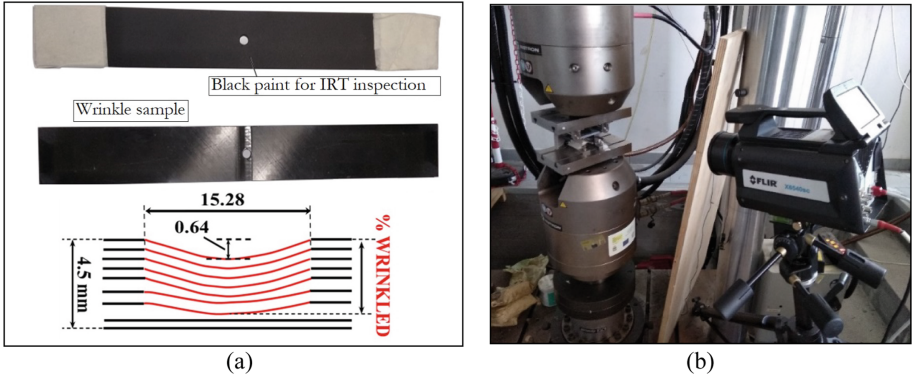


**Fig. 1.** (a) Surface preparation for ND monitoring approaches and schematic view of wrinkled zone of W-type elements; (b) experimental and thermographic setup of B-type samples.

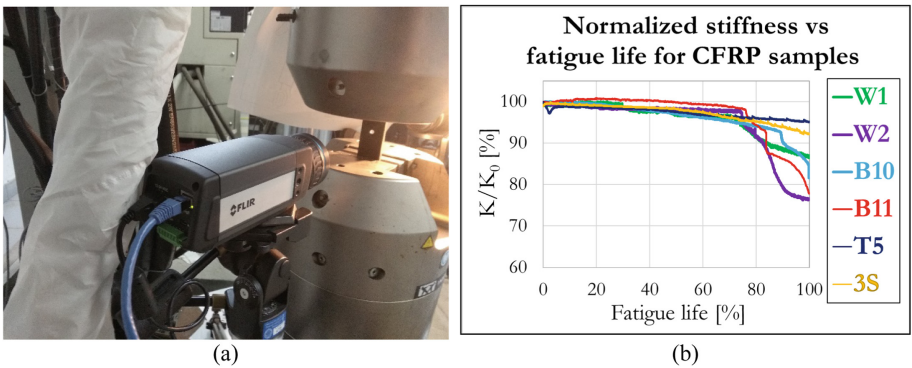


**Fig. 2.** (a) experimental and monitoring setup of OHT ‘T-S’ samples for fatigue damage evaluation with IR and digital cameras; (b) Normalized stiffness curves vs fatigue life for CFRP series.

IMS-(0) carbon fiber and Prism TM EP2400 Liquid epoxy toughened resin and manufactured with rectangular cross section through Liquid Resin Infusion process, with fiber volume fraction of about 48–49%.

Finally, the last CFRP elements consist of composite samples with OHT configuration as shown in Fig. 2 (a). This composite batch (denoted ‘T-S’ type) includes two flat samples [Dim. 177.8 × 28.8 × 6.55 mm] with a central hole of 4.74 mm with countersink 2 × 45°, realized in autoclave to reproduce tensile fatigue behaviour in presence of hole for aeronautic bolted junctions. These specimens consist of 20 woven fabrics of thickness 0.327 mm with a stacking sequence of [±45, 0/90, 0/90, 0/90, ±45]<sub>2s</sub> symmetrically arranged. Delamination initiations, matrix cracking and finally fiber breakage are observed through fatigue cycles in ‘T-S’ series, in the layers at the onset of countersunk region.

For each CFRP series, preliminary static tests were performed for each test cases to evaluate the reference ultimate load ( $F_{static}$ ) and relative displacement ( $u_{static}$ ), employed

**Table 1.** Scheduled experimental results for CFRP elements.

| ID CFRP element |     | Stress ratio | Load frequency [Hz] | F <sub>Amp_norm</sub> [%] | N. fatigue cycles [N <sub>f</sub> ] | Damage zone and type                             |
|-----------------|-----|--------------|---------------------|---------------------------|-------------------------------------|--|
| Wrinkle samples | W1  | 0.1          | 8                   | 17.42                     | 101,617                             | Crack 1° layer; delamination 6° layer            |
|                 | W2  |              |                     | 16.85                     | 370,173                             | Crack 1° layer; delamination 6° layer            |
| Beam samples    | B10 | 0.05         | 4                   | 29.48                     | 13,289                              | Delamination in 10° ply                          |
|                 | B11 |              |                     | 24.02                     | 66,911                              | Delamination in 6° and 10° layers                |
| 'T-S' samples   | 5T  | 0.1          | 9                   | 93.88                     | 318,797                             | Crack and delamination around countersunk layers |
|                 | 3S  |              |                     | 91.66                     | 737,481                             | Crack and delamination around countersunk layers |

to define subsequent cyclic loads, whose fatigue parameters and main resulting data are reported in Table 1, with  $F_{Amp\_norm}$  the semi-amplitude load related to  $F_{static}$  and different indications of relative damaged zones. All static and cyclic tests are performed in displacement and load control mode respectively on the servo - hydraulic INSTRON 8850 axial-torsion test machine, equipped with a load cell of  $\pm 250$  KN, as illustrated in Fig. 1(b). Selected sample surfaces are preventively covered with a high-temperature black paint for thermal monitoring procedure, as shown in Fig. 1(a).

For W-type and B-type samples, thermal data are acquired during fatigue endurance employing a cooled IR camera FLIR X6540sc (Flir System), selecting a frame rate of 117 Hz and observation time of 10 s. Concerning the 'T-S' samples, a micro-bolometer FLIR A655sc thermal camera is employed for fatigue monitoring, recording thermal signals at regular fatigue intervals with a frame rate of 100 Hz and observation time of 10 s. Specific thermographic set-ups are optimized in terms of distance sample-camera for a suitable control monitoring of regions of interest of samples, as shown in Fig. 1(b) and Fig. 2(a) for 'B'-type and 'T-S' type respectively.

In fatigue test, the specimen stiffness variation is commonly employed to express the damage state of polymer composites and a cumulative damage DK parameter is defined

as [11]:

$$D_K = (1 - K/K_0) * 100 \quad (1)$$

where  $K$  and  $K_0$  represent the actual and initial stiffnesses, respectively. The experimental results include the compliance analysis where the stiffness behaviour is evaluated during all fatigue life until final failure.

## 2.2 Thermal Damage Parameters

In literature, different authors demonstrate that thermal dissipation could be related to damage progression and TSA based approach could be successfully employed as an indicator of damage accumulation during fatigue loading [7, 11]. Thermal variation in terms of amplitude oscillation is related to reversible thermoelastic heating and cooling during cycling loads [11]. In fact, during cyclic loading conditions, the material volume always followed by heat releases and a part of energy necessary to damage propagation transformed in an irreversible heat source [12]. Several authors proposed different thermoelastic approaches successfully applied for rapid estimation of the fatigue limit of homogeneous or orthotropic materials in stepwise cyclic tests with increasing stress amplitude levels [13, 14].

An alternative TSA analytical model allow to extract thermal signal information from thermographic sequences acquired during each fatigue test. In particular, the thermal signal is processed in the time domain based on following equation [14]:

$$T(i, j, t) = T_0 + b * t + T_{the} * \sin(\omega * t + \pi + \varphi) + A * \cos(2 * \omega * t + \psi) \quad (2)$$

where the sum  $\mathbf{T}_0 + \mathbf{b} * \mathbf{t}$  (denoted as  $\mathbf{T}_{sum}$ ) describes the mean increase in the average dissipative thermal signal during fatigue test;  $\omega$  is the angular frequency with which the imposed load signal varies;  $\mathbf{T}_{the}$  and  $\varphi$  are respectively the amplitude and the phase of first harmonic component related to thermoelastic signal;  $\mathbf{A}$  and  $\psi$  represent respectively the second component amplitude and the phase of thermal signal obtained at a double frequency [14]. Algorithm allow to extract the various signal information from each selected ROI to obtain as output six ( $\mathbf{T}_0$ ,  $\mathbf{b}$ ,  $\mathbf{T}_{the}$ ,  $\mathbf{A}$ ,  $\varphi$  and  $\psi$ ) signal parameter reported in Eq. (2), evaluated during fatigue tests.

The aim of this study consists of different fatigue damage evaluation, introducing TSA contrast parameters based on reversible and irreversible thermoelastic sources. In fact, different methods are proposed in case of ND control thermographic inspections to provide enhancing contrast for defect detection and to reduce various noises and other error sources [13, 14]. Thermal processing techniques lie in thermal contrast evaluation, comparing relative temperature behavior during observation time in selected Regions of Interest (ROIs) in different defective and defect-free zones. In this work, the research focus lies on the possible introduction of a TSA contrast-based method for the cumulative damage identification and quantification in an established zone. Based on thermoelastic theory, a first normalized Thermoelastic Contrast parameter could be performed for specific damage evaluation from reversible heating source during the fatigue life ( $N_{tot}$ ) as:

$$D_{rev}(N) = \left( \left[ (\Delta T/T) / (\Delta T/T)_0 \right]_d - \left[ (\Delta T/T) / (\Delta T/T)_0 \right]_i \right) * 100 \quad (3)$$

where  $(\Delta T/T)_d$  and  $(\Delta T/T)_i$  represent the TSA ratio for damaged and undamaged regions (ROIs) at a given time of fatigue life ( $N/N_{tot}$ ). Each ratio is normalized respect to the same relative TSA ratio at initial fatigue life, respectively. Specifically, the terms  $\Delta T$  and  $T$  represent the thermal variations and temperature averaged over the selected ROIs during fatigue observation time ( $N/N_{tot}$ ), respectively. In addition, assuming initially undamaged conditions, the cumulative damage zone elated to dissipative heat release could also provide interesting information on material degradation. The authors propose an alternative damage analysis coefficient to the previous one, to be evaluated in function of fatigue life ( $N/N_{tot}$ ) with a second parameter:

$$D_{diss}(N) = [(T/T_0)_d - (T/T_0)_i] * 100 \quad (4)$$

where the thermal values represent the average temperatures over the same ROIs at given fatigue time ( $N/N_{tot}$ ). This  $D_{diss}$  parameter represents damage progression associated with a normalized contrast evaluated with temperature ratio of the mean load level in selected damaged and undamaged zones respectively.

Then, each sequence of 3D thermal ROIs is post-processed in MATLAB environment following Eqs. (3) and/or (4) as function of fatigue life and compared with stiffness behaviour. For each CFRP sample, the authors optimize experimental monitoring setups to achieve a suitable ROI of the most critical zones where interesting thermal data, displacement fields and in-situ deformations could arise. The reference intact zones are selected calculated in several ROIs without recorded significative variations on the proposed damage factors. However, since the damage presented multiple defective spots due to widespread delamination and matrix cracking. Therefore, a group of almost five defective and defect-free ROIs are evaluated for the assessment of damage parameters, selected in critical zones where damage initiation could be observed during fatigue life.

### 3 Results and Discussion

Preliminary compliance analysis is performed for three CFRP series at selected stress ratio. Comparative analysis of percentage stiffness behavior as function of normalized fatigue life is presented in Fig. 2(b) for each composite element. In this diagram, stiffness variation is reported as function of fatigue life under different cyclic loads, where the stiffness data (denotated as  $\mathbf{K}$ ) were normalized to specific stiffness initial value ( $\mathbf{K}_0$ ) and number of cycles to relative total fatigue cycles. Before fatigue damage, both curves of W-type samples show an almost stabilized general trend in the initial phase to central part, followed by a rapid stiffness decay before failure. Generally, 75% of total fatigue life is ensured with small compliance increment, before significative matrix cracking and delaminations start to spread until sudden failure, with collapse of wrinkled specimen sides, when internally induced macro defects could be propagated in the critical central section length. A rapid decay during the final phase of fatigue life is observed for W2 element before failure, with a severe stiffness reduction of 35%. In B-type test cases, a further rapid reduction suddenly appears in the stiffness trends between 70 ÷ 90 of fatigue life, as observed in Fig. 2(b) due to higher level of applied cyclic loads. Finally, stiffness data of T5 element highlight a slow decreasing trend during initial and intermediate test phase, achieving a final stiffness degradation around 5% at 90 ÷ 100% of fatigue life.

Instead, higher stiffness degradation is reached by 3S sample, whose fatigue data show a clear continuous decreasing trend from 0% to 50 ÷ 60% of fatigue life, when a severe stiffness degradation is observed until a decrease of 7 ÷ 8% before the final fatigue failure.

Therefore, MATLAB processing codes are employed on selected ROIs for the quantitative comparison of damage initiation and progressive evolution between different tested specimens during relative fatigue life. By Eq. (2) to (4), five TSA coefficients and two damage ( $D_{diss}$ ,  $D_{rev}$ ) parameters could be established respectively to provide different and complementary information related to material damage state.

For wrinkle elements, three damage parameters and thermo-elastic  $T_{the}$  or dissipative  $A$  coefficients are evaluated in output processed maps during fatigue life in selected ROIs with a couple of zones representative of damaged zones and the other couple related to reference undamaged areas.

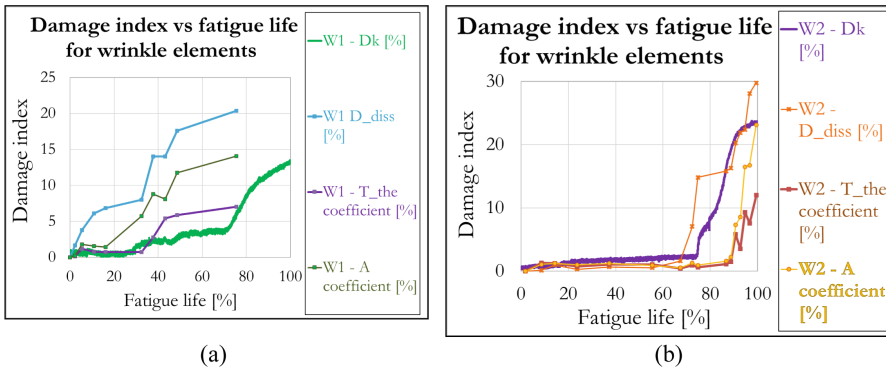


Fig. 3. (a) Fatigue parameters vs fatigue life for W1 and (b) W2 samples.

As shown in Fig. 3(a) and Fig. 3(b), damage parameters data and TSA coefficients trends are reported for two damaged W-type elements as function of normalized fatigue life. A trend variation could be observed at almost at 75% of fatigue life showing a similar behavior of relative  $D_K$  stiffness parameter due to progressive damage accumulation before final failure. Resulting  $D_{diss}$  curves seem to provide slightly higher data than relative  $D_K$  parameters, whose results seem to reach different percentages results around 10 ÷ 30%. An almost stabilized general trend is shown in the initial phase to central part in all curves for W2 element shows a rapid data increasing after the 70% of fatigue life. Therefore, the compliance analysis represents a robust reference start-point for data evaluation of different processing techniques.

Concerning the B-type elements, during fatigue tests, thermographic monitoring acquisitions highlight a full-field different stress increasing that creates between layers' different heat generation increasing the temperature from reference undamaged image as function of fatigue life. Therefore, normalized profiles are selected in two central areas (one in upper layers and other one in bottom layers) and evaluated during fatigue life for both B-type specimens. For quantitative analysis, average TSA coefficient values are estimated in selected zones by processed output maps and examples  $T_{the}$  and  $A$



variations parameters are reported as function of normalized fatigue life in Fig. 4. In the diagrams of normalized TSA coefficients, an evident variation in the thermos-elastic and dissipative mechanical response between tensile and compressed layers could be detected in B10 and B11 samples, tested under higher loading conditions.

Both TSA profiles highlights evident variation trend for compressive zones and zones subjected to tensile stress where an evident variation of second harmonic’s amplitude could be observed during 37% of fatigue life in B10 sample due to damage growth before final failure, as shown in black line of Fig. 4 (a–b). Evident delamination occurrence is clearly distinguished generally only in the last cycles and for several specimens, whilst clear indications of damage nucleation are observed in B10 and B11 samples. This is probably due to severe loading conditions or also to composite micro-structure under localized bending supports. Therefore, comparative analysis between damage parameter  $D_{rev}$  and  $D_{diss}$  evaluated for two ROIs of B-type samples as function of normalized fatigue life are reported in Fig. 5 (a–c) and discussed.

Similar behaviour is observed between the curves in both diagrams, where the  $D_{rev}$  and  $D_{diss}$  parameters both provide an evident decreasing after an initial increasing of relative data and a clear trend variation observed at 50% of fatigue life, probably due of progressive damage accumulation before final failure and delamination initiation induced also in tensile ROIs. In Fig. 5 (b), these curves seem to indicate a more severe damage of tension zones than the compressed areas.

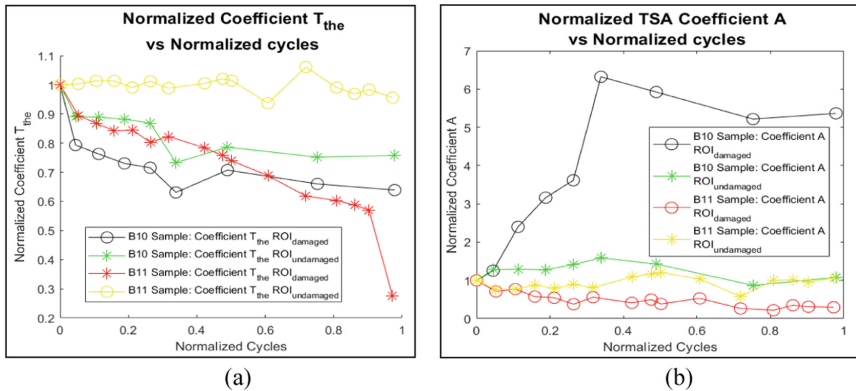


Fig. 4. (a) Normalized TSA Coefficient  $T_{the}$  and (b)  $A$  vs fatigue life for B10 and B11 elements.

Finally, the quantitative analysis, in Fig. 6 (a–b), the processed thermal profiles as function of during fatigue life respectively are reported for selected CFRP elements to evaluate damage initiation in terms of damage parameters based on stiffness degradation ( $D_K$ ), reversible ( $D_{rev}$ ) or dissipative sources ( $D_{diss}$ ) measurements.

The comparative analysis of damage parameters provides different diagrams of resulting data based on TSA sources at different fatigue cycles for each sample series. Specifically,  $D_{rev}$  data show high level of noise (scattering) and a certain trend variability due to ROI choice has been noted, but parameter values seem to increase in each specimen. As observed, it appears that  $D_{rev}$  behavior follows the damage regime



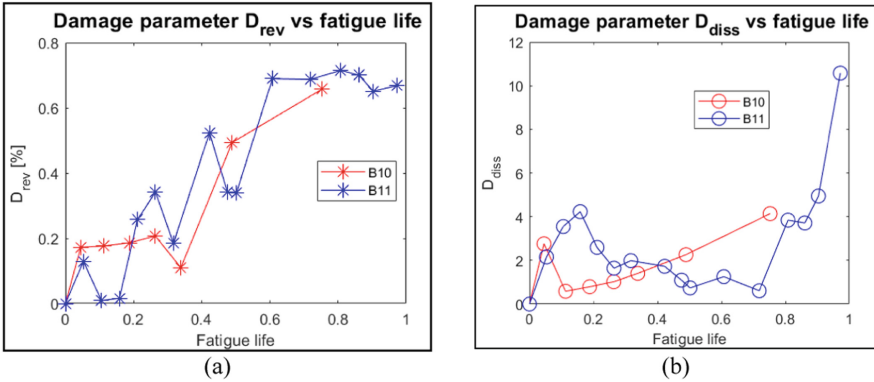


Fig. 5. (a) Diagrams of  $D_{rev}$ , (b)  $D_{diss}$  vs fatigue life for B-type elements.

even if it suffers a lot of noise and critical damage propagation is clearly distinguished, highlighting similar behavior between 5T and 3S samples.

In general, the  $D_{rev}$  parameter seems characterized by an initial phase, that starts from 20% of fatigue life without an evident growth of parameter trend, and by a second phase, where an evident curve growth over one value seems to occur at 50–55% life in ‘T-S’ specimens’ series. Instead, as shown Fig. 6(b),  $D_{diss}$  data show a damage evolution with an approximately exponential trend with foible data variability, highlighting similar trend behavior with stiffness degradation  $D_K$  parameters.

Therefore, assuming initially undamaged conditions, the proposed damage parameter evaluated by  $D_{diss}$  data seems to provide an interesting behavior highlighting the 5% data variation before the cumulative damage  $D_K$  profiles related to stiffness degradation, validating initial assumptions on raw damage initiation proposal, based on TSA approach, implemented according to contrast-based method.

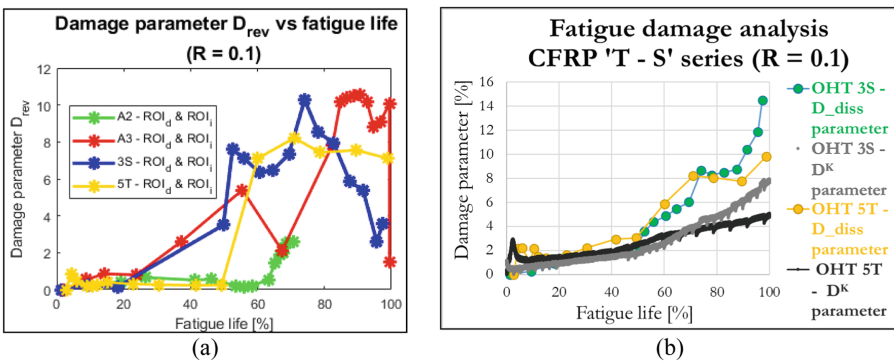


Fig. 6. (a) Diagram  $D_{rev}$  and (b)  $D_K$  and  $D_{diss}$  parameters vs fatigue life for CFRP ‘T-S’ series.

## 4 Conclusions

The damage initiation is not easy to be detected in composite elements during fatigue loading conditions. Therefore, in this proposed study, the authors provide to perform a suitable full-field monitoring and post-processing procedures for a proper damage initiation and progression on different CFRP elements under cyclic loads.

Specifically, two contrast-based parameters denoted as  $D_{rev}$  and  $D_{diss}$  are proposed for damage prediction assessment and related to thermoelastic reversible and dissipative effects, respectively. The comparative analysis between the stiffness degradation and the post-processed thermal results obtained using different approaches is discussed for three composite series. An interesting correlation is observed between proposed damage parameters respect to stiffness results and TSA post-processed data. Comparative analysis seems to highlight satisfactory results for fatigue damage prediction through the proposed damage parameters.

## References

1. Timmis, A.J., et al.: Environmental impact assessment of aviation emission reduction through the implementation of composite materials. *Int. J. Life Cycle Assess.* **20**(2), 233–243 (2014). <https://doi.org/10.1007/s11367-014-0824-0>
2. Scelsi, L., Bonner, M., Hodzic, A., et al.: Potential emissions savings of lightweight composite aircraft components evaluated through life cycle assessment. *Expre Polym. Lett.* (2011). <https://doi.org/10.3144/expresspolymlett.2011.20>
3. Boursier Niutta, C., Tridello, A., Paolino, D.S., Belingardi, G.: Residual properties in damaged laminated composites through nondestructive testing: a review. *Materials* **14**, 4513 (2021). <https://doi.org/10.3390/ma14164513>
4. Sohn, H., et al.: A Review of Structural Health Monitoring Literature 1996—2001; Los Alamos National Laboratory, Los Alamos, pp. 1–303 (2004)
5. Duchene, P., Chaki, S., Ayadi, A., Krawczak, P.: A review of non-destructive techniques used for mechanical damage assessment in polymer composites. *J. Mater. Sci.* **53**(11), 7915–7938 (2018). <https://doi.org/10.1007/s10853-018-2045-6>
6. Kralovec, C., Schagerl, M.: Review of structural health monitoring methods regarding a multi-sensor approach for damage assessment of metal and composite structures. *Sensors* **20**(3), 826 (2020). <https://doi.org/10.3390/s20030826>
7. Pitarresi, G., Cappello, R., Catalanotti, G.: Quantitative thermoelastic stress analysis by means of low-cost setups. *Opt. Lasers Eng* **134**, 10615 (2020). <https://doi.org/10.1016/j.optlaseng.2020.106158>
8. Vassilopoulos, A.P., Keller, T.: Experimental characterization of fiber-reinforced composite materials. In: *Fatigue of Fiber-Reinforced Composites*. Springer, London, pp. 25–67 (2011). [https://doi.org/10.1007/978-1-84996-181-3\\_2](https://doi.org/10.1007/978-1-84996-181-3_2)
9. Middleton, C.A., McCrory, J.P., Greene, R.J., Holford, K., Patterson, E.A.: Detecting and monitoring cracks in aerospace materials using post-processing of TSA and AE Data. *Metals* **9**(7), 748 (2019). <https://doi.org/10.3390/met9070748>
10. Thatcher, J., Crump, D., Devivier, C., Bailey, P., Dulieu-Barton, J.: Low-cost infrared thermography for automated crack monitoring in fatigue testing. *Opt. Lasers Eng.* **126**, 105914 (2020). <https://doi.org/10.1016/j.optlaseng.2019.105914>
11. Toubal, L., Karama, M., Lorrain, B.: Damage evolution and infrared thermography in woven composite laminates under fatigue loading. *Int. J. Fatigue* **28**, 1867–1872 (2006). <https://doi.org/10.1016/j.ijfatigue.2006.01.013>

12. Chrysochoos, A.: Infrared thermography, a potential tool for analyzing the material behaviour. *Méc. Ind.* **3**(1), 3–14 (2002)
13. La Rosa, G., Risitano, A.: Thermographic methodology for rapid determination of the fatigue limit of materials and mechanical components. *Int. J. Fatigue* **22**(1), 65–73 (2000). [https://doi.org/10.1016/S0142-1123\(99\)00088-2](https://doi.org/10.1016/S0142-1123(99)00088-2)
14. Galietti, U., Demelio, G.P., Palumbo, D., De Finis, R.: A new rapid thermographic method to assess the fatigue limit in GFRP composites. *Compos B.* **103**, 60–67 (2016). <https://doi.org/10.1016/j.compositesb.2016.08.007>